

# Pre- and Post-Failure Experimental Bending Analysis of Glass Elements Coated by Aged Anti-Shatter Safety Films

**Silvana Mattei, Luca Cozzarini, Chiara Bedon**

University of Trieste, Italy, [chiara.bedon@dia.units.it](mailto:chiara.bedon@dia.units.it)

## Abstract

The main goal of Anti-Shatter Films (ASFs) applications for structural glass is to create a barrier able to keep together fragments and minimize risk after any impulsive or static load that could lead glass to cracking. The influence of ASF properties on the flexural strength of coated glass elements is thus a relevant topic for safe design purposes, but still little investigated. To this aim, an experimental material investigation is presented in this paper, in order to achieve a good knowledge of common ASFs from a chemical point of view. Moreover, the deterioration of mechanical and adhesion characteristics for ASF samples subjected to different environmental conditions and accelerated ageing is also investigated, so as to simulate the effects of long-term exposure to high humidity (HU) or high temperature (HT). An experimental campaign carried out on 20 small scale ASF-coated glass specimens is finally presented, based on a three-point bending (3PB) test setup. The out-of-plane bending response of unaged or aged samples is performed by taking into account two different displacement-rate levels, to assess their performance and bending capacity under steady-static or impulsive loads. In both cases, the attention is given to the characterization of elastic and post-failure performances. Finally, support for the interpretation of experimental outcomes is derived from a simplified theoretical model of composite beam with partial connection, in order to estimate the shear stiffness of ASF adhesive components in the elastic stage.

## Keywords

Three-point bending (3PB), Accelerated ageing, Anti-Shatter Film (ASF), Experiments, Post-failure behaviour

## Article Information

- Digital Object Identifier (DOI): [10.47982/cgc.8.401](https://doi.org/10.47982/cgc.8.401)
- This article is part of the Challenging Glass Conference Proceedings, [Volume 8](#), 2022, Belis, Bos & Louter (Eds.)
- Published by [Challenging Glass](#), on behalf of the author(s), at [Stichting OpenAccess Platforms](#)
- This article is licensed under a [Creative Commons Attribution 4.0 International License](#) (CC BY 4.0)
- Copyright © 2022 with the author(s)

## 1. Introduction

Anti-Shatter Safety Films (ASFs) are typically used in practice to mitigate the consequences of glass breakage. The first applications can be found in the early 1970s by British Government, in order to lessen the effects of terrorist bombing. Thanks to the impressive results, the use of ASFs began to expand in different fields of application. Meanwhile, the improvement in choice of materials and / or manufacturing technologies were developed by companies interested in the versatility of the product. Nowadays, there are several anti-shatter glass films on the market, almost all transparent offering invisible protection in case of an accident, thus against shattering, breaking, explosions or vandalism. Therefore, it is crucial to assess and quantify the efficiency and benefits for different application surfaces. Although this kind of commercial products have passed several standard certification tests as reported in the Guidance Note (2013), the poor literature in experimental experiences that provide a measure of the increasing glass system strength (Ahn 2019; Kojima et al. 2021; Memari et al. 2004; Van Dam et al. 2014) should be improved. Generally, to reduce or avoid risks structural robustness can be provided in glass constructions by using redundancy at different levels. Several studies were aimed at mechanical characterization of laminated glass plate subjected to bending loading with different interlayers (Serafinavicius et al. 2013) or environmental temperatures (Antolinc 2020) or progressive damage (Biolzi et al. 2010). The main advantage of laminated glass is its capacity to act as safety glass, due to section redundancy, in different areas such as for windshields in the automobile industry (Batzer et al. 2007) or classical façade components (Weggel et al. 2008). Therefore, most of the studies conducted on the bending behaviour and the impact response of glass have focused on laminated sections, due to their ability to remain substantially intact (Castori et al. 2017; Iwasaki et al. 2007; Sable et al. 2017; Timmel et al. 2007). Alternatively, the major disadvantage of architectural float glass is the lack of residual strength, so generally fracture corresponds to sudden collapse.

In this regard, the present experimental study is focused on the investigation of the out-of-plane bending behaviour of aged monolithic glass specimens fitted with ASFs, analysing both the elastic and the post-fracture phases. Two accelerated ageing protocols are employed, exploring the influence of high temperature and humidity on the adhesion performance, as also in accordance with (Butchart & Overend 2017). The resistance improvement for glass element is a fundamental topic in a vulnerability analysis with regard to natural causes, such as earthquakes, hurricanes, etc., and even accidental events. The assessment of ASF-coated glass behaviour in out-of-plane bending is hence carried out in this paper via three-point bending (3PB) test setup, with both a quasi-static or impact regime. For the plane elastic problem, theoretical expressions are developed by considering shear phenomena at the interface between glass substrate and PET-film. Finally, the basic material characterization and mechanical capacity for the tape and ASF-coated samples is discussed.

## 2. Theoretical analysis

Generally, the mechanical coupling of two or more structural elements in out-of-plane bending takes place through the use of special connection systems (i.e., composite slabs, columns, beams, etc.). These connections, both discrete or continuous, have the task of resuming the sliding effort between the linked elements, in order to transmit an axial effort between them. In the field of structural glass applications, typical examples include adhesive linear bonds for hybrid beams (Louter 2011; Firmo et al. 2020; etc.).

In the same way, the contribution of ASF in the out-of-plane bending behaviour of coated glass elements can be taken into account thanks to the presence of PSA, whose possibility of providing a residual resistance is analysed in this study. The reference composite system can be seen in Fig. 1, where subscript “1” and “2” are related to the glass element and the PET-film respectively.

In doing so, a basic important approximation is made in considering the absence of peeling phenomena until the complete detachment, which corresponds to the loss of strength in the test procedure.

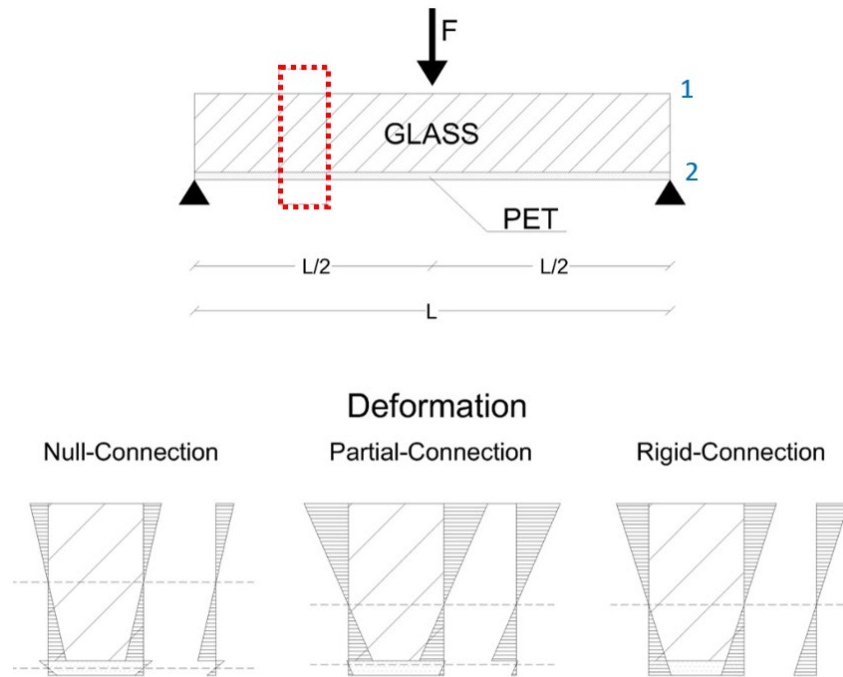


Fig. 1: Qualitative layout of out-of-plane bending deformation for ASF-coated glass element, as a function of shear connection behaviour.

Since the efficiency of the composite structural element is higher when the shear stiffness of the connection is high, the smaller are the displacements relative to the interface of the two elements. Typically, the real connection behaviour is intermediate between zero and infinite stiffness (Fig. 1). In the former case, the two elements are simply in parallel; considering Bernoulli’s hypothesis valid, the pane sections of the individual component beams are preserved. Instead, in the latter case, the two bonded components are rigidly coupled together and the overall section of composite system deforms as homogeneous one, with no sliding at the interface. Additionally, the constitutive law of these connectors is rarely linear, and may suffer for degradation due to ageing.

According to original Newmark’s theory (1951), for intermediate conditions of partially rigid connection and relative sliding as in Fig. 1, the real behaviour of the composite beam can be reduced to the response of two elements bending in parallel and connected by a deformable connection with elastic-linear stiffness  $K$ . The solution by Newmark is valid for a simply supported beam made up of a maximum of two different layers. Furthermore, in this discussion several hypotheses are considered, such as (i) uniformly distributed connection along the span, (ii) constant geometries / section properties, (iii) linear elastic behaviour of materials and (iv) same curvature for elements “1” and “2”. Adaptations of Newmark’s analytical model for laminated glass elements can be found for example in (Amadio & Bedon 2010; Amadio & Bedon 2011) for extension to buckling-related aspects.

On the basis of above assumptions, and through some simplification and integration steps, it is possible to arrive at the equation of composite beam as in Fig. 1, able to describe the bending deformation  $v(x)$ :

$$v(x) = c_1 \frac{x^2}{2} + c_2 \frac{e^{\alpha^2 x}}{\alpha^4} + c_3 x + c_4 - \alpha^2 \frac{M}{EJ_{full}} \frac{x^3}{6} - \frac{1}{2\alpha^4} \frac{M}{J_{full}} \frac{e^{2\alpha^2 x}}{2\alpha^2} \quad (1)$$

with:

$$\alpha^2 = \frac{K}{EA^*} \frac{EJ_{full}}{EJ_{abs}} \quad (2)$$

$$K = \frac{G_{ad} b}{t_{ad}} \quad (3)$$

$M$  is the bending moment to which the beam is subjected,  $t_{ad}$  is the stiffness of the adhesive and  $G_{ad}$  is the tangential stiffness of PSA. The coefficient  $\alpha$  is function of the equivalent axial stiffness  $EA^*$ , the bending stiffness  $EJ_{full}$  (determined in the hypothesis of rigid shear connection between elements "1" and "2") and the bending stiffness  $EJ_{abs}$  (as in absence - or very weak - shear connection). These equivalent terms can be calculated as:

$$EA^* = \frac{E_1 A_1 \times E_2 A_2}{E_1 A_1 + E_2 A_2} \quad (4)$$

$$EJ_{abs} = E_1 J_1 + E_2 J_2 \quad (5)$$

$$EJ_{full} = EJ_{abs} + EA^* d \quad (6)$$

### 3. Experimental program

The present study aims to analyse the out-of-plane bending response of ASF-coated glass elements by investigating the influence of temperature and humidity on its key mechanical parameters. The experimental campaign consisted of 20 three-point bending (3PB) tests on glass elements fitted with ASF and 15 uniaxial tensile tests on PET.

In particular, the flexural bending tests covered two imposed deformation rates, thus resulting in low speed (0.5 mm/min) and high speed (1 m/min) experiments respectively, so as to analyse the response under impulse. Moreover, to characterise the influence of individual components, a study was carried out on the mechanical characteristics of PET to quantify the effects of temperature and humidity variations on the elastic modulus of this material.

#### 3.1. Materials characterization

The ASF material under investigation was selected to coincide with a commercially available multi-layer film. Special attention was paid to detect the differences in tensile behaviour after ageing (film only) and in out-of-plane bending behaviour (when coupled to glass). All glass elements were provided by the same factory and manufactured by annealing process.

The examined multi-layer tape is sketched in Fig. 2. As shown, the typical ASF is composed of three different layers (0.11 mm in thickness) bonded together by an interposed adhesive, and a PSA adhesive to ensure contact with glass substrate. The latter is usually protected by environmental conditions by means of a removable release liner.

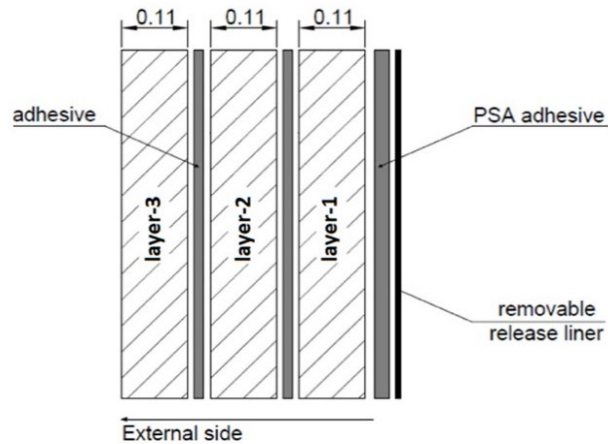


Fig. 2: Stratification detail for the examined multi-layer ASF (measures in mm).

The layer material as well as the adhesives were investigated by Fourier Transform Infrared spectroscopy (FT-IR) and Differential Scanning Calorimetry (DSC). FT-IR is a technique that allows investigating the chemical nature of materials by analysing the vibrational bands associated to different functional groups. DSC is a thermal analysis technique that evaluates the heat exchange difference between sample and reference as a function of temperature and time. In the case of crystalline or semi-crystalline materials, information on the melting and crystallization temperature and enthalpy associated with phase change can be obtained.

As shown in Fig. 3, FT-IR spectra of layer-1, layer-2 and protective liner (acquired on both sides) and internal side of layer-3 show vibrational bands consistent with polyethylene terephthalate (PET) (Socrates 2004). FT-IR spectrum of external side of layer-3 show different vibrational bands, overlapping those typical of PET: this are consistent with an amine. Surface treatments of PET with such compounds are often used as stabilizers or UV absorbers (Aflori et al. 2007; Rusu et al. 2008).

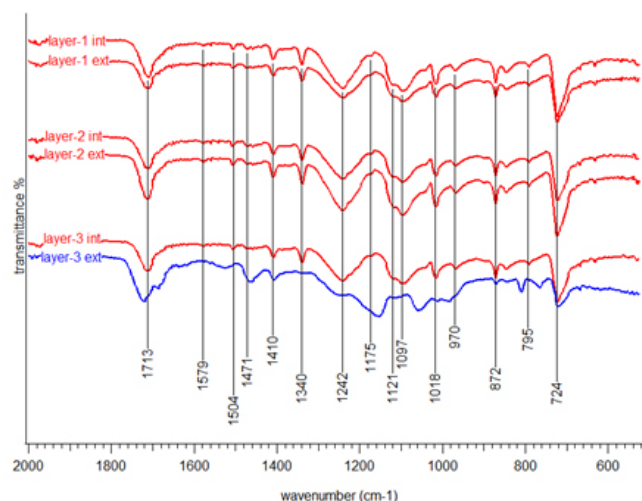


Fig. 3: FT-IR spectra of layer 1,2 and 3. Layers 1 and 2 (both sides) and layer-3 (internal side) spectra show good match with PET vibrational bands (vertical lines). Spectrum of layer-3, external side (blue curve) shows some minor difference respect to PET vibrational bands due to extra vibrational band ascribable to an amine surface treatment.

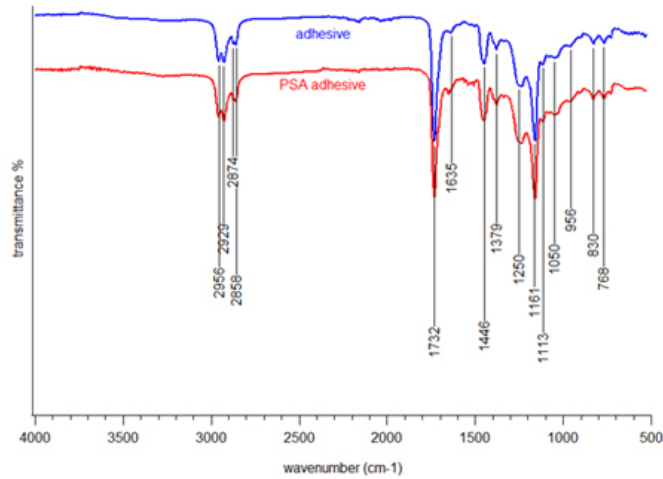


Fig. 4: Vibrational bands identified on the adhesive between the layers and on the PSA adhesive.

FT-IR spectra of the adhesive between the layers and that of PSA adhesive are identical (i.e., Fig. 4), pointing out that the adhesives share the same chemical composition. Vibrational bands identified CH<sub>3</sub>, CH<sub>2</sub>, C-O-C and C=O groups; the overall spectrum is consistent with that of a poly ethyl acrylate or poly allyl acrylate (often used as PSA adhesive), see for example (Mapari et al. 2021; Marquez et al. 2020).

FT-IR spectra of layers and adhesive after ageing processes do not show any difference respect to unaged sample spectra. This implies that no chemical degradation (oxidation) took place on PET layers and that no degradation or cross-link reaction occurred in the adhesive during the ageing processes.

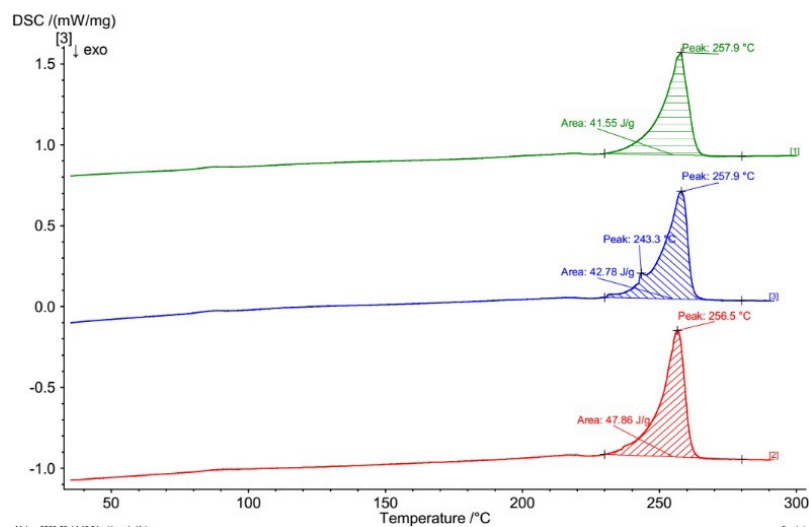


Fig. 5: DSC heating thermograms of layer-1 (green), layer-2 (blue) and Layer-3 (red).

Thermograms of layer-1 (green curve), layer-2 (blue curve) and layer-3 (red curve) are shown in Fig 5. All heating curves show a primary melting point around 257°C (with melting enthalpy of 40-50 J/g); these values are consistent with the typical values found in literature for semicrystalline PET (CES Selector database 2012; Polymer Data Handbook 1999). Layer-2 show also a secondary melting peak at 243°C: the presence of a second polymer, blended with the PET, could be speculated. Polybutylene terephthalate (PBT) and poly trimethylene terephthalate (PTT) are often used in PET/PBT and PET/PTT

blends (Liu et al. 2013; Piccinini et al. 2013; Son et al. 2003) and their melting temperature is consistent with this secondary melting peak.

### 3.2. Test specimens and setup

As shown in Fig. 6, the reference sample size of 100 mm x 40 mm x 6 mm and 100 mm x 40 mm x 0.35 mm (length x width x height) were considered for glass and ASF respectively in 3PB tests. Details of the setup of the bending tests are also shown in Fig. 7. Tests were performed with a Shimadzu AGS-X universal testing machine; the span between the lower supports was set to 64 mm.

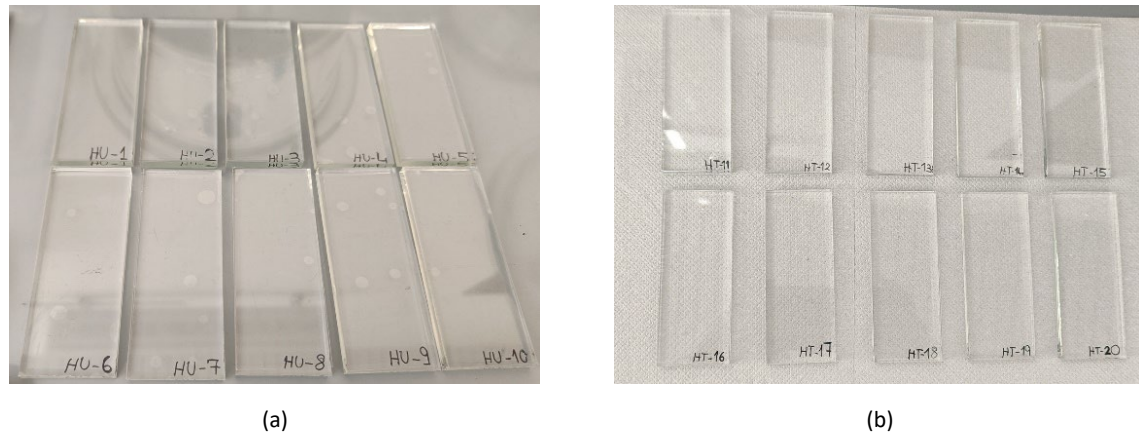


Fig. 6: ASF-coated glass specimens: (a) HU and (b) HT ageing procedures.

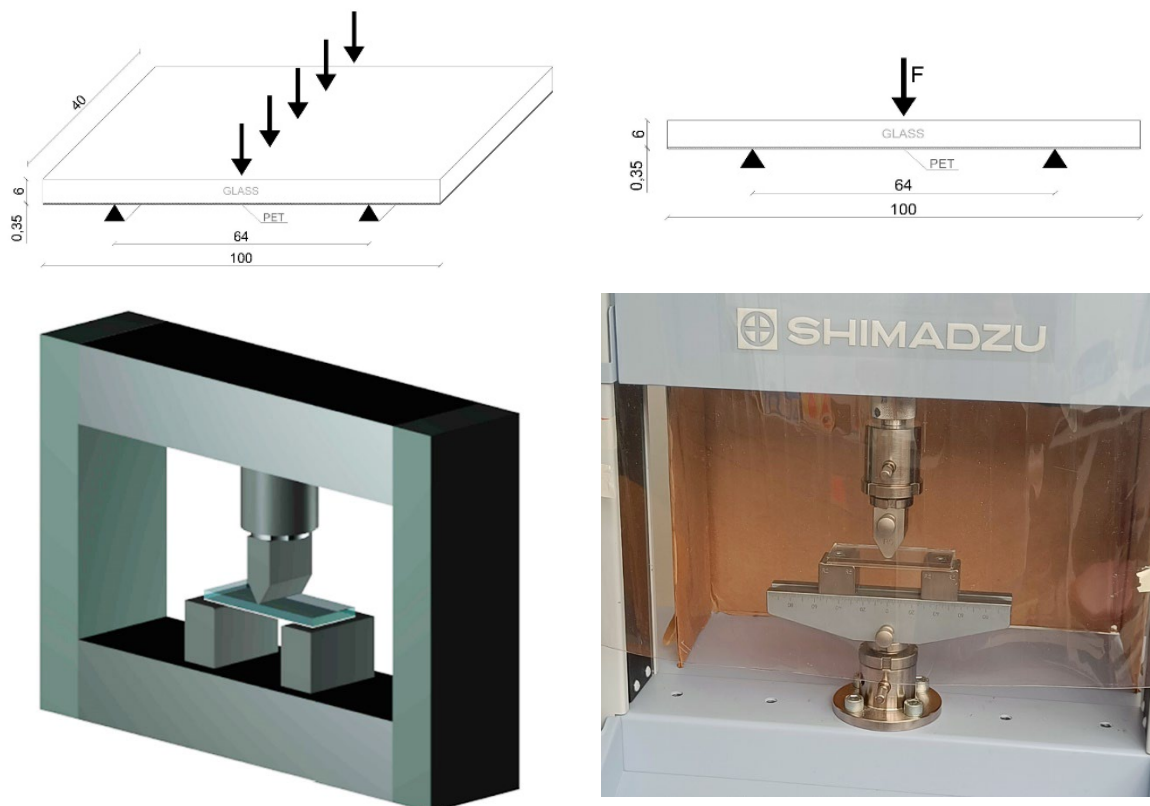


Fig. 7: Set-up of Three-Point Bending tests (measures in mm).

A crosshead speed of 0.5 mm/min was used for low speed tests (10 specimens), 1 m/min for high speed tests (10 specimens). This latter high displacement rate was applied in order to evaluate the flexural strength before cracking and its residual value thanks to the presence of ASF. However, in both cases the crack initiation and propagation process in the glass was very fast and rather difficult to monitor. The span between the supports was 64 mm. The diameter of 5 mm characterized both loading apparatus, equipped with a load cell, and the steel supports along their entire width.

The experimental data (force, displacement) were automatically recorded for each time step using a data acquisition system, where the load was applied at the midspan through a fixed displacement rate but different for two sets of specimens:

- low-speed rate for HU-i and HT-j, with  $i=1$  to 5 and  $j= 11$  to 15;
- high-speed rate of for HU-i and HT-j, with  $i=6$  to 10 and  $j= 16$  to 20.

Regarding tensile tests, specimens of clean PET-film with the same geometry (200 mm x 25 mm x 0.34 mm) such as represented in Fig. 8, were tested by means of tensile tests with a Shimadzu AGS-X universal testing machine, with a crosshead speed of 25.4 mm/min at room temperature (Fig. 9). These were tested to characterize the mechanical properties of the tape material without any interferences of the PSA; they were obtained after removing the PSA with a suitable solvent (acetone, specifically chosen to be able to dissolve PSA but be inert towards PET). Moreover, an interesting investigation on tensile properties on each layer was performed after separating the layers composing the PET tape and testing them individually with the same parameters (crosshead speed of 25.4 mm/min).



Fig. 8: PET-film specimens: (a) HU and (b) HT ageing procedures.

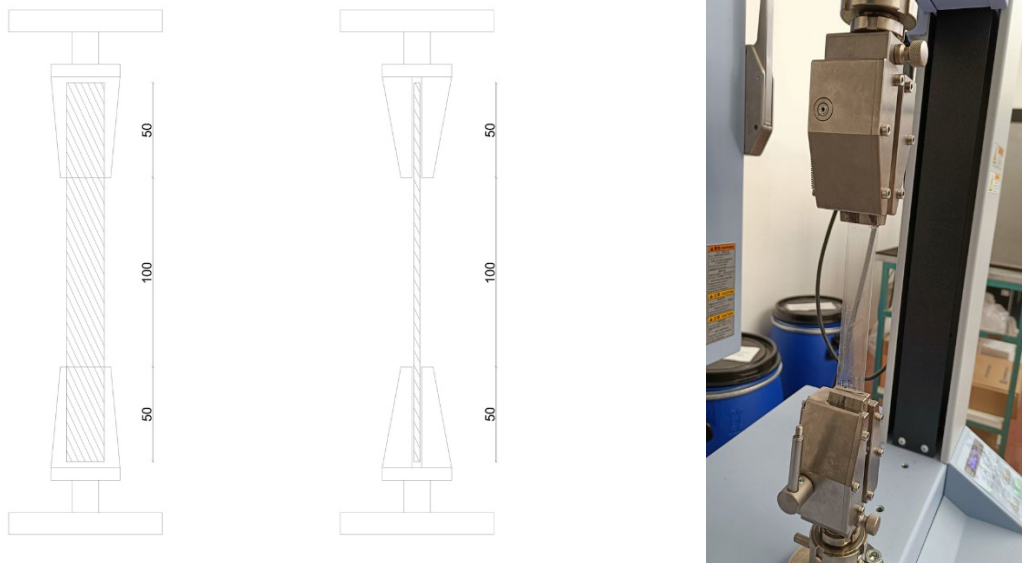


Fig. 9: Set-up of PET-film tensile tests (measures in mm).

### 3.3. Ageing procedures

Two accelerated ageing procedures were investigated in order to simulate the effects of long-term exposure to high humidity (HU) and high temperature (HT) environments, according to EN 12543-4 that is specifically developed for identification of glass laminates (with PVB, EVA or SG) durability. In HU procedure specimens were held in a vacuum box in a vertical position over water for a period of 2 weeks within the limit of 50°C, while in HT procedure specimens were heated in a convection oven to 100°C for a period of 120 minutes. Subsequently, the tests were performed within a limit of 3 hours.

## 4. Experimental results and discussion

Stress-strain curves of tensile tests performed on clean PET material are shown in Fig. 10. Stress-strain curves of each layer are shown in Fig. 11. The evaluation of the tensile test of the PET tape was preparatory to the analysis of the flexural response of the composite section (glass + adhesive + PET). The main goal of this test was the comparison of results in terms of mean modulus of elasticity ( $E_2$ ) between the three sets, that is unaged and aged specimens (based on HU and HT ageing procedures respectively). The load-displacement curves of tensile tests for PET tape showed a very similar qualitative behaviour before and after aging; as shown in Fig. 10 (b), there was no discernible difference in  $E$  values (3.3 GPa the average), giving evidence of high consistency with previous analyses on similar components (Mattei et al. 2022).

With respect to the individual films, it can be noticed in Fig. 11 that the average moduli of elasticity of the single layers are slightly greater than the actual value of the overall unaged section.

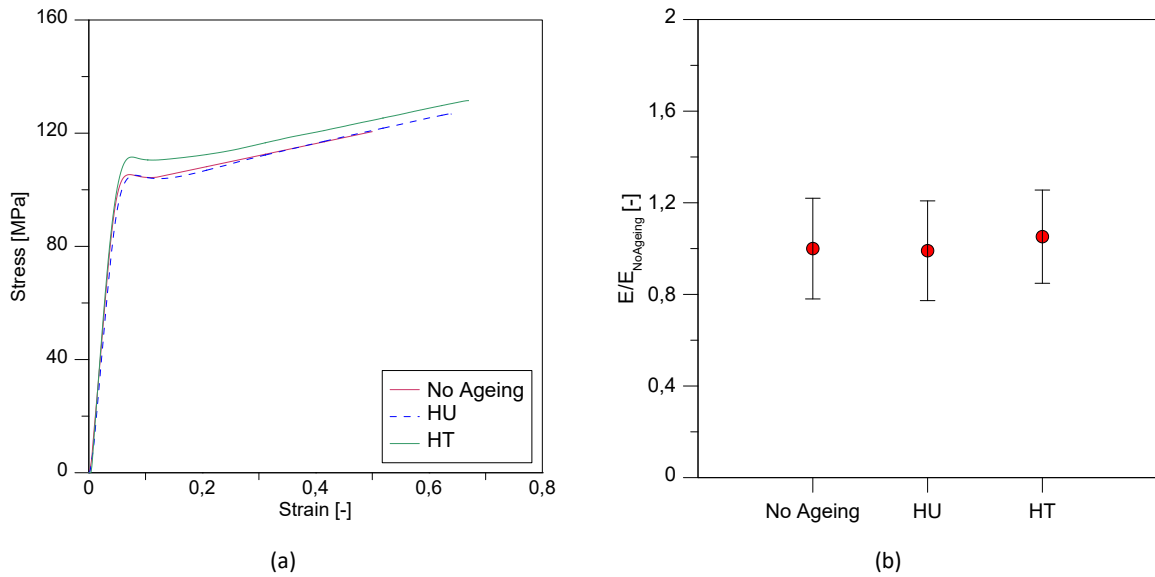


Fig. 10: (a) Stress-strain curves at different ageing conditions. (b) E normalized to the unaged value.

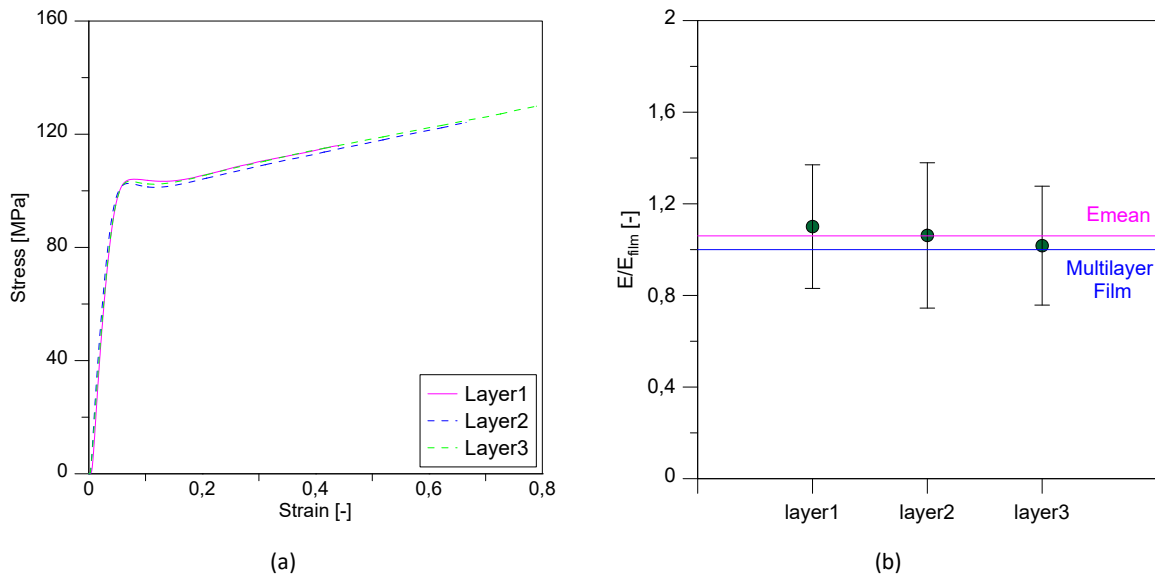


Fig. 11: (a) Stress-deformation curves of each layer. (b) Young's modulus, E, of each layer normalized to the one of the overall film

The load-displacement curves of the low-speed 3PB tests, carried out on “glass+film” system, are depicted in Fig. 12. The first part of the curves was elastic-linear, generally until the maximum force value representing the glass failure ( $F_{break}$ ) was reached; after this point, an abrupt reduction in strength was detected, followed by a segment in which a residual value of strength ( $F_{residual}$ ) was recorded, most likely due to the presence of the ASF. Finally, the last portion of the load-displacement curves, after the second sudden strength loss, corresponds to the film's contribution alone following the complete detachment of the adhesive layer on one or both bottom sides of specimens caused by the opening of cracks. Monolithic brittle materials, such as annealed glass, are known for the typical sudden failure, which usually occurs in the elastic region. The benefit of having a residual strength, provided by safety films, is one of the main aspects which lead to the choice of using this type of tool to increase the post-breakage behaviour of float glasses. In order to evaluate the influence of ASF on the bending behaviour of the glass element, an analysis of  $F_{break}$  and  $F_{residual}$  values was performed, and the relative results

were summarized in Table 1. The variation observed between the maximum load values before the fracture, represented by the standard deviation reported, is due to the non-uniform behaviour of glass that depends by many factors, such as manufacturing technique, edge defects, chemical composition and crack pattern (i.e., Fig. 13). As a consequence, it should be noted that the crack distribution typically concentrated around the midspan but the position of initiation cracking point and the number of cracks change. However, HU-1 curve was neglected in the evaluation of the parameters reported in Table 1 because it involves singular values, also supported by a different crack pattern (i.e., Fig. 12(a)). The findings summarized in Table 1 are reflected in the Fig. 12: the exposure to HU ageing led to an increase of interfacial adhesion and, consequently, of ratio  $F_{residual}/F_{break}$  with a corresponding increase in displacement at failure. However, the exposure to HT ageing provides better results than the previous one in terms of residual strength and maximum displacements until the overall collapse.

Table 1: Summary of experimental outputs from 3PB tests (average  $\pm$  standard deviation).

Specimen	$F_{break}$ [N]	$F_{residual}$ [N]	$F_{residual}/F_{break}$ [-]	$F_{max}$ [N]	$K_{el}$ [mJ]
HU-2 / HU-5	800 $\pm$ 540	110 $\pm$ 20	0.13	-	77 $\pm$ 17
HT-11 / HT-15	1040 $\pm$ 240	460 $\pm$ 80	0.44	-	125 $\pm$ 52
HU-6 / HU-10	-	-	-	330 $\pm$ 160	608 $\pm$ 275
HT-16 / HT-20	-	-	-	480 $\pm$ 100	726 $\pm$ 196

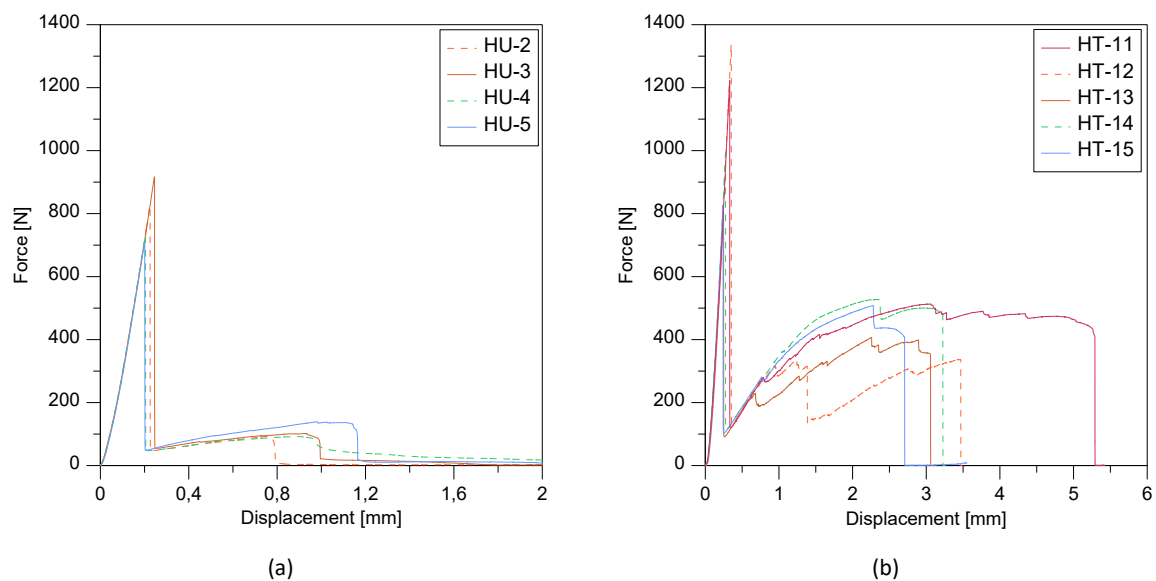


Fig. 12: Load-displacement curves at low-speed rate: analysis of experimental results based on ageing protocols with (a) High Humidity or (b) High Temperature.

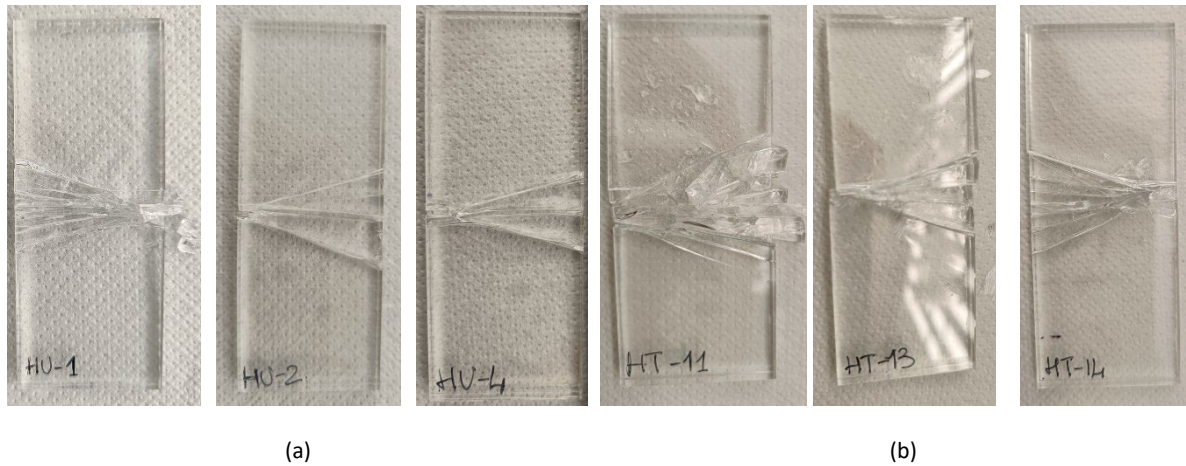


Fig. 13: Post-failure crack pattern of (a) HU specimens and (b) HT specimens (selection).

Based on the theoretical background by Section 2, a numerical parametric analysis was performed in order to calculate the tangential stiffness of the adhesive layer related to the elastic phase, by imposing  $v(L_0/2) = v_{exp}$ . Where  $v_{exp}$  represents the displacement recorded during the 3PB tests by testing machine and  $v(L_0/2)$  corresponds to the theoretical solution by Eq. (1) in the same region.

Moreover, Fig. 14 shows tensile stresses evaluated at the bottom surface of the glass,  $\sigma_{1,max}$  (in the hypothesis of rigid connection) and at the bottom surface of the film,  $\sigma_{2,max}$ , in the midspan section corresponding to the maximum bending moment  $FL_{span}/4$ :

$$\sigma_{1,max} = \frac{M}{J} y_1 \quad (7)$$

$$\sigma_{2,max} = n \frac{M}{J} y_2 \quad (8)$$

with  $n$  the ratio between the modulus of elasticity of PET and glass ( $n = E_2/E_1$ ).

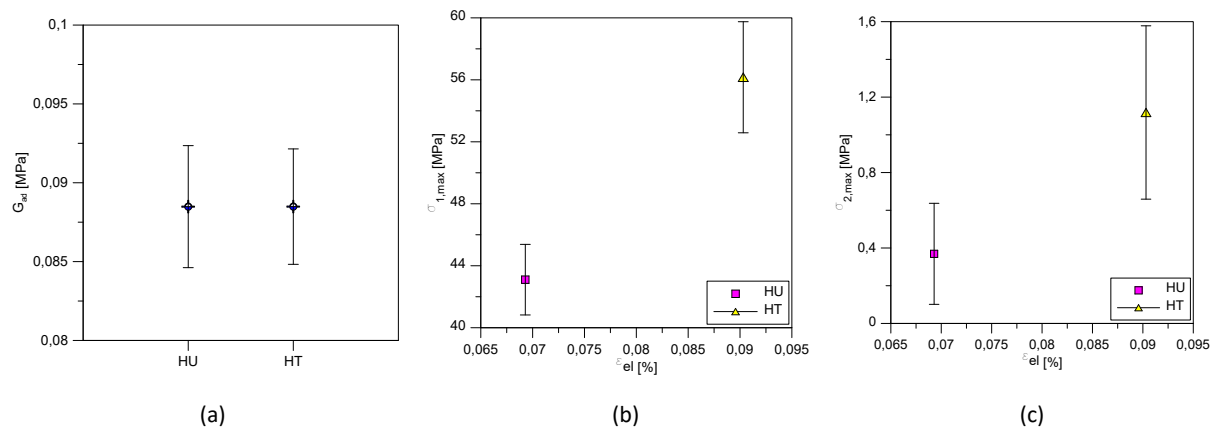


Fig. 14: (a) Tangential stiffness of PSA. (b)  $\epsilon_{el} - \sigma_{1,max}$ . (c)  $\epsilon_{el} - \sigma_{2,max}$  with respect to the both ageing procedures.

The investigation of the tests results was done by discussing the effects of the ASF on the mechanical behaviour of monolithic glass. A further analysis on the post-breaking branch was focused to build an equivalent numerical model able to calculate the residual strength and deflection taking into account that the section does not crack but that the tangential stiffness of the adhesive decreases following a power-law, as reported in Fig. 15. Although the trend of the two curves appears to be the same, the

curve for the specimens aged at high humidity reflects the experimental evidence showing a higher rate of decrease of the parameter  $G$ .

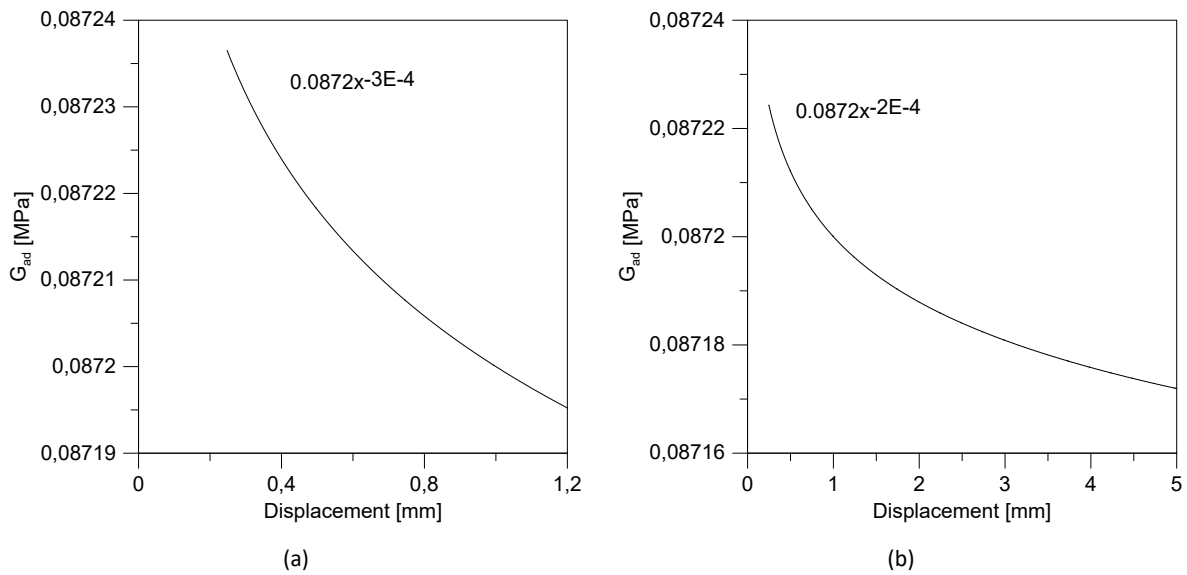


Fig. 15: Power-law for (a) HU-specimens and (b) HT-specimens.

For the high-speed 3PB tests, the load-displacement curve presents a completely different shape as shown in Fig. 16. In this case the analysis of the results was performed in terms of equivalent strain energy, or absorbed energy in impact bending, computed as the area under the load-deflection curve up to the peak force, related to the onset of the first crack. This parameter corresponds to the toughness ( $K_{el}$ ) of the linear region reported in the last column of the Table 1 and in Fig. 17 (a). Furthermore, another benchmark for comparison of the bending behaviour in different ageing conditions can be  $F_{max}$  as reported in Fig. 17 (b). It can be noted that the HT ageing procedure provided a greater load-carrying capacity in the elastic and post-brakeage phases for low-speed rate 3PB test, and greater tensile toughness and maximum force in case of  $v= 1$  m/min.

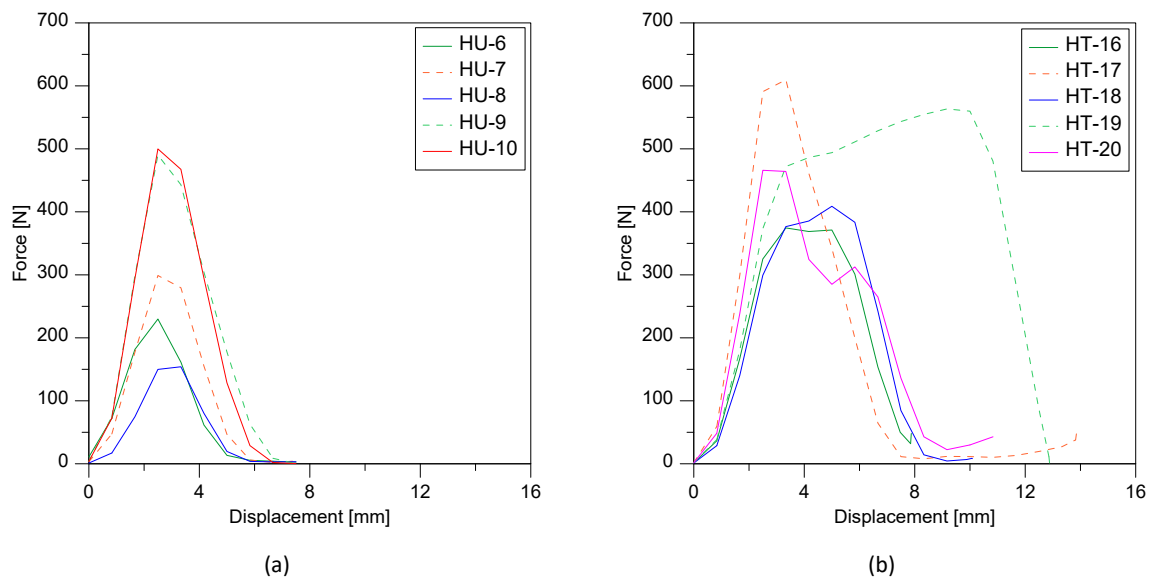


Fig. 16: Load-displacement curves at high-speed rate: Ageing protocols (a) High Humidity and (b) High Temperature.

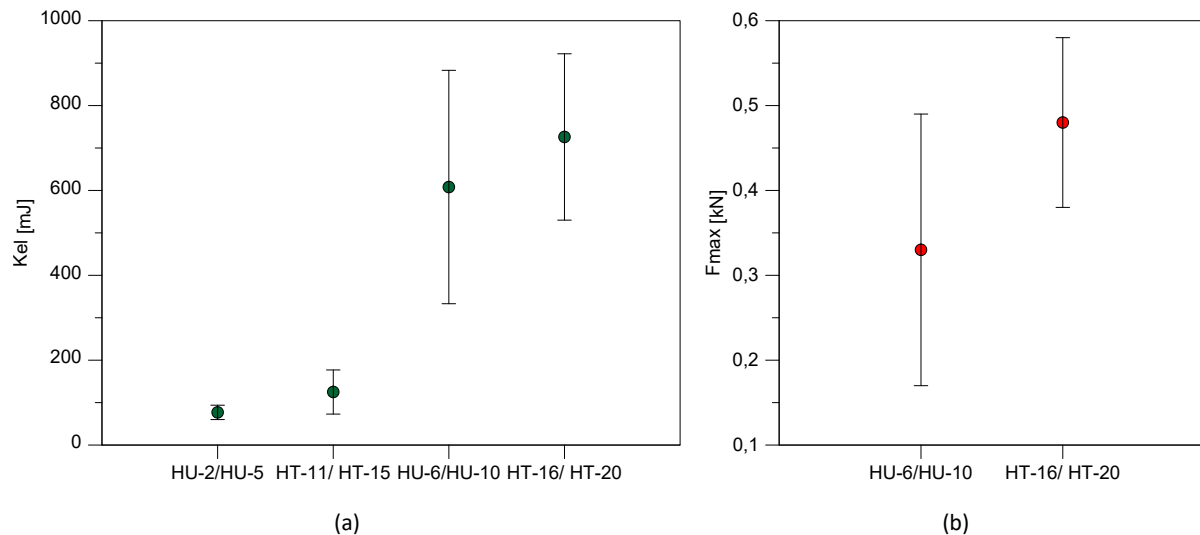


Fig. 17: (a) Toughness of the linear region,  $K_{eI}$  and (b) maximum value of force,  $F_{max}$ .

## Summary and conclusions

As noticed, the maximum bending force and midspan deflection at failure under three-point bending test highlights the uncertainties involved in the glass breakage process. Both accelerated ageing procedures considerably affected flexural strength of coated glass specimens. Therefore, the behaviour of specimens after cracking is totally influenced by the PET-film adhesion characteristics, thanks to which the remaining fragments held together by the tape express a little residual strength and a deformation at collapse, recorded at  $L_0/2$ , greater than twice that related to cracking. In particular, comparison of the environment influence showed that the selected conditioning methods affected the adhesion performance and thus the bending response of the “glass+ASF” composite system.

By a chemical point of view, the pre-conditioning with the accelerated ageing procedures does not involve any modification in the components. Moreover, there are no major differences in failure mechanisms between the four sets of specimens. In qualitative terms, the force-displacement response was affected by viscosity property of the PSA, and in particular of the tackifier resin which improve its wettability to the adherent and accelerate the adhesive bonding to the substrate.

Of course, all ageing conditions investigated in this work caused a change in the post-breakage branch: the exposure to high humidity for two weeks provided about  $0.1F_{break}$  as residual strength, and the exposure to high temperature showed higher values of peak forces and just over 40% as a residue. In this latter case, the tape increased ductility feature beyond the linear-elastic phase. Conversely, with a high-speed rate tests flexural response didn't show a post-fracture curve. Therefore, the displacement-rate influence was assessed in terms of dissipated energy as strain and computed as the area under the curve up to the peak value. Furthermore, the ageing on PET-film mechanical parameter were found to be of negligible influence by mean tensile tests. This paper highlights the need for further study that take into account tangential and normal stress components at the interfacial surface by including the delamination process in the theoretical treatment.

## Acknowledgements

This research study was financially supported by University of Trieste (“Microgrants 2020” grant).

The ongoing EU COST Action CA18120 “CertBond” is also acknowledged for facilitating research networking and discussion of present topic by authors with international experts. Finally, Seretti Vetroarchitetture is acknowledged for providing glass samples.

## Conflict of interest

The authors declare there is no conflict of interest with the publication of this manuscript.

## References

- Aflori, M., Drobotă, M., Timpu, D., Barboiu, V.: Amine functionality of poly (ethylene terephthalate) films surfaces induced by chemical and RF plasma treatments. 28th ICPIG, topic 13, 727-730 (2007).
- Ahn, K.C.: Impact response of the film mechanical properties of the coated glass plate. *Int. J. Mech. Prod. Eng. Res. Dev.*, 9(2), 499-506 (2019).
- Amadio, C., Bedon, C.: Buckling of Laminated Glass Elements in Compression. *Journal of structural Engineering*, 137(8), 2011
- Amadio, C., Bedon, C.: Buckling of laminated glass elements in out-of-plane bending. *Engineering Structures*, Volume 32, Issue 11, November 2010, Pages 3780-3788
- Antolinc, D.: Three-point bending test of laminated glass with PVB and EVA interlayers at elevated temperature. In: Belis, J., Bos, F., Louter, C., (eds.) *Conf. Archit. Struct. Appl. Glass CGC 2020 – Proc.*
- Batzer, S.A., Thorbole, C.K., Herndon, G.G., Beltran, D.: Injury analysis of laminated and tempered side glazing. *The Engineering Institute United States*, 07-0101 (2007).
- Biolzi, L., Cattaneo, S., Rosati, G.: Progressive damage and fracture of laminated glass beams. *Constr. Build. Mater.*, 24, 577-584 (2010).
- Butchart, C., Overend, M.: Influence of Aging on Post-Fracture Performance. *Proceedings of Glass Performance Days Conference* (2017).
- Castori, G., Speranzini, E.: Structural analysis of failure behavior of laminated glass. *Compos. B. Eng.*, 125, 89-99 (2017).
- Centre for the Protection of National Infrastructure - GUIDANCE NOTE: PEEL ADHESION TESTING AND ASSESSMENT OF ANTI-SHATTER FILM (ASF), (2013).
- Firmo, F., Jordao, S., Costa Nees, L., Bedon, C.: Exploratory study on simple hybrid or pre-stressed steel-glass I-beams under short-term bending – Part 1: Experiments. *Composite Structures*. Volume 234, 15 February 2020, 111651
- GRANTA Design, CES Selector Software Materials Data Set (2012).
- Iwasaki, R., Sato, C., Lataillade, J.L., Viot, P.: Experimental study on the interface fracture toughness of PVB (polyvinyl butyral)/glass at high strain rates. *Int. J. Crashworthiness*, 12, 293-298 (2007).
- Kojim, T., Suzuki, M., Notomi, M.: Numerical simulation on dynamic fracture of glass plate fitted with a polymeric film. *Adv. Mat. Res.*, 1166, 57-64 (2021).
- Liu, F., Yao, M., Run, M.: Synthesis and Characterizations of Poly(trimethylene terephthalate)-b-poly(tetramethylene glycol) Copolymers. *Int. J. Polym. Sci.*, 156289 (2013). [dx.doi.org/10.1155/2013/156289](https://doi.org/10.1155/2013/156289).
- Louter, C.: *Fragile yet Ductile. Structural Aspects of Reinforced Glass Beams*. PhD Thesis, TU Delft, The Netherlands; 2011.
- Mapari, S., Mestry, S., Mhaske, S.T.: Developments in pressure-sensitive adhesives: a review, *Polymer Bulletin* 78, 4075-4108 (2021). <https://doi.org/10.1007/s00289-020-03305-1>.
- Marquez, I., Alarcia, F., Velasco, J.L.: Synthesis and Properties of Water-Based Acrylic Adhesives with a Variable Ratio of 2-Ethylhexyl Acrylate and n-Butyl Acrylate for Application in Glass Bottle Labels, *Polymers*, 12(2), 428 (2021). <https://doi.org/10.3390/polym12020428>.
- Mattei, S., Cozzarini, L., Bedon, C.: Experimental and numerical peeling investigation on aged multi-layer anti-shatter safety films (ASFs) for structural glass retrofit. *Symmetry*, 14(1), 162 (2022).
- Memari, A.M., Behr, R.A., Kremer, P.A.: Dynamic racking crescendo tests on architectural glass fitted with anchored pet film. *J. Archit. Eng.*, 10(1), 5-14 (2004).

- Newmark, N.M., Siess, C.P., Viest, I.M.: Tests and analysis of composite beams with incomplete interaction. *Proc. Soc. Exp. Stress Anal.*, 9(1), 75–92 (1951).
- Piccinini, P., Senaldi, C., Alberto Lopes, J.F: Fibre Labelling Poly(trimethylene terephthalate) - PTT- DuPont. Publications Office of the European Union (2013). doi:10.2788/82737.
- Polymer Data Handbook 2nd ed., Oxford Press (1999).
- Rusu, E., Drobota, M., Barboiu, V.: Structural investigations of amines treated polyester thin films by FTIR-ATR spectroscopy. *J. Optoelectron. Adv. Mater.*, 10, 377–381 (2008).
- Sable, L., Skukis, E., Japins, G., Kalnins, K.: Correlation between numerical and experimental tests of laminated glass panels with visco-elastic interlayer. *Procedia Eng.*, 175, 945-952 (2017).
- Serafinavicius, T., Kevedaras, A.K., Sauciuvėnas, G.: Bending behavior of structural glass laminated with different interlayers. *Mech. Compos. Mater.*, 49(4), 437-446 (2013).
- Socrates, G.: Infrared and Raman characteristic group frequencies: tables and charts, John Wiley & Sons (2004).
- Son, Y.S., Ji, D.S.: Synthesis and hydrophilicities of Poly(ethylene 2,6-naphthalate)/Poly(ethylene glycol) copolymers. *Fibers Polym.*, 4, 20-26 (2003). doi.org/10.1007/BF02899325.
- Timmel, M., Kolling, S., Osterrieder, P., Du Bois, P.A.: A finite element model for impact simulation with laminated glass. *Int. J. Impact Eng.*, 34, 1465-1478 (2007).
- Van Dam, S., Pelfrene, J., De Pauw, S., Van Paepegem, W.: Experimental study on the dynamic behaviour of glass fitted with safety window film with a small-scale drop weight set-up. *Int. J. Impact Eng.*, 73, 101-111 (2014).
- Weggel, D.C., Zapata, B.J.: Laminated glass curtain walls and laminated glass lites subjected to low-level blast loading. *J. Struct. Eng.-ASCE*, 134, 466-477 (2008).

## CertBond - COST Action CA18120

This paper was presented as part of a special session organised at Challenging Glass Conference 8 by the [CertBond Cost Action CA18120](#) “Reliable roadmap for certification of bonded primary structures”.



## Platinum Sponsors

---

The Eastman logo, consisting of the word 'EASTMAN' in a bold, red, sans-serif font.

## Gold Sponsors

---

The Bellapart logo, featuring the word 'Bellapart' in a bold, blue, sans-serif font.The kuraray logo, featuring the word 'kuraray' in a blue, lowercase, sans-serif font.The Trosifol logo, featuring the word 'Trosifol' in a black, sans-serif font with a registered trademark symbol.The SentryGlas logo, featuring the words 'SentryGlas' in a black, sans-serif font with a registered trademark symbol.The sedak logo, featuring the word 'sedak' in a bold, black, lowercase, sans-serif font.

## Silver Sponsors

---

The octatube logo, featuring the word 'octatube' in a bold, italicized, black, sans-serif font.The vitroplena structural glass solutions logo, featuring a blue stylized 'v' icon above the text 'vitroplena structural glass solutions' in a black, sans-serif font.

## Organising Partners

---

The TU/e logo, featuring the text 'TU/e' in a bold, red, sans-serif font.The TU Delft logo, featuring a black stylized flame icon above the text 'TU Delft' in a bold, black, sans-serif font.